Dielectric formulation of strongly coupled electron liquid at metallic densities. III. Dynamic structure factor

Kenichi Utsumi and Setsuo Ichimaru
Department of Physics, University of Tokyo, Bunkyo-ku, Tokyo 113, Japan
(Received 23 September 1980)

Dynamic structure factor of strongly coupled electron liquid at metallic densities is calculated theoretically on the basis of the general dielectric formulation and the numerical evaluation of the static structure factor presented in previous papers. The results are compared with the experimental data for Al and other metals on a number of specific points such as the plasmon dispersion curve both below and above the critical wave number, the plasmon linewidth, and asymmetry of the excitation spectrum. Overall features of the calculated excitation spectrum show substantially improved agreement with the experimental indications, with a notable exception that the theory does not account for the double-peak structure observed in some experiments. A theoretical expression for the plasmon dispersion coefficient is presented, which encompasses many of the existing formulas as its limiting cases; comparison with the experimental values is also given.

I. INTRODUCTION

During the past decades, a substantial amount of effort has been expended on the experimental study of the dynamic structure factor associated with the valence electrons in metals, through the techniques of x-ray scattering spectroscopy and electron energy-loss spectroscopy.[1–15] The dynamic structure factor refers to the spectral function of the density-fluctuation excitations in such an electron system.[16] The experiments have revealed the frequency dispersion, the linewidth, and the spectral shape of the plasmon excitations, as well as the detailed features of the contributions coming from other elementary excitations.

In various instances, the theory on the basis of the random-phase approximation[17] (RPA) has failed to account for salient features observed in experiments. Such a discord has been anticipated, however, since the RPA is basically a weak-coupling theory. The electrons in metal are on the contrary a strongly Coulomb-coupled system, for which the coupling constant r_s is greater than unity. Many investigators[18–23] have attempted to go beyond the RPA description, by taking account of certain non-RPA effects arising from the exchange and Coulomb correlations. Those theories have achieved only limited success in comparing their numerical predictions with the experimental data.

In our previous paper,[24] hereafter referred to as I, we have formulated a dynamic theory of strongly coupled electron liquids at metallic densities. The dielectric response function $\epsilon(q,\omega)$ so obtained contains three characteristic functions: the local-field correction $G(q)$, the relaxation time in the long-time region $\tau(q)$, and the relaxation frequency in the short-time domain $\Omega(q)$. Each of those functions describes a strong-coupling effect due to the exchange and Coulomb interactions; it is thus expressed as a functional of the static structure factor. In a subsequent paper,[25] hereafter referred to as II, we have then numerically solved the resulting set of the self-consistent integral equations for the static structure factor; the static and thermodynamic properties of such electron liquids have thereby been investigated.

In this paper we extend the work described in I and II, and now carry out explicit computations of the dynamic structure factor for the electron liquids at metallic densities. By doing so, we wish also to clarify the extent to which the experimental results may be understood within the framework of such an electron-liquid theory. The overall features of the excitation spectrum calculated in this paper appear to agree fairly well with the experimental results; a notable exception, however, lies in the fine structure of the spectrum where some experiments[5] have found double-peak characters. Such an overall accuracy of the present theory is expected, since the original formalism in I satisfies a number of integrated relations such as the frequency-moment sum rules.

In Sec. II, we briefly review the formulations developed in I and II, in such a way that the computational procedures of the dynamic structure factor are established. In Sec. III, we consider a phenomenological treatment of the extra collisional

effects due to those physical processes other than the electron-electron interactions in the liquid; we thereby introduce the corresponding rate of momentum transfer and investigate its effects on the plasmon dispersion and linewidth. The results of numerical computations for the plasmon dispersion and the dynamic structure factor are presented and compared with the experimental data in Sec. IV. Findings of this paper are summarized in Sec. V. Since this work is a continuation of I and II, we closely follow the notation and convention adopted in those papers unless otherwise specified.

II. DYNAMIC STRUCTURE FACTOR

The dynamic structure factor $S(q,\omega)$ is related to the dielectric response function $\epsilon(q,\omega)$ via the fluctuation-dissipation theorem,[16] i.e.,

$$S(q,\omega)=-\left[\frac{\hbar V}{\pi v(q)}\right]\mathrm{Im}\left[\frac{1}{\epsilon(q,\omega)}\right]\quad(\omega>0)\ . \tag{1}$$

Here $v(q)=4\pi e^2/q^2$ is the Coulomb interaction and V refers to the volume of the system. According to Eq. (3.12) in I, the dielectric function is expressed as

$$\epsilon(q,\omega)=1-\frac{v(q)(\tilde{\omega}/\omega)\chi_0(q,\tilde{\omega})}{1+\{v(q)(\tilde{\omega}/\omega)G(q)+[(\tilde{\omega}-\omega)/\omega\chi_0(q,0)]\}\chi_0(q,\tilde{\omega})}\ , \tag{2}$$

where

$$\tilde{\omega}=\omega+\left[\frac{2}{\pi}\right]^{1/2}\frac{\Omega(q)}{\omega\tau(q)}\left[W\left(\frac{\omega}{\Omega(q)}\right)-1\right]\ , \tag{3}$$

$$W(z)=\frac{1}{(2\pi)^{1/2}}\int_{-\infty}^{\infty}dx\ \frac{x}{x-z-i\eta}\exp\left[-\frac{x^2}{2}\right] \tag{4}$$

is the plasma dispersion function, and $\chi_0(q,\omega)$ represents the Lindhard polarizability[26] as given in Eq. (3.22) of I.

The static local-field correction $G(q)$ has been evaluated in II as a sum of the exchange contribution $G_{ex}(q)$ and the remaining Coulomb contribution $G_c(q)$. The former has been expressed as Eq. (30) in II; the latter takes the form,

$$G_c(q)=-N^{-1}\sum_{k\neq\vec{0},\vec{q}}K(\vec{q},\vec{k})S_{WS}(k)\times[S(|\vec{k}-\vec{q}|)-S_{HF}(|\vec{k}-\vec{q}|)]\ . \tag{5}$$

Here N is the total number of electrons,

$$K(\vec{q},\vec{k})=\vec{q}\cdot\vec{k}/k^2+\vec{q}\cdot(\vec{q}-\vec{k})/|\vec{q}-\vec{k}|^2 \tag{6}$$

is the symmetrized Coulomb interaction, and $S_{HF}(q)$ refers to the static structure factor in the Hartree-Fock approximation [see Eq. (35) in II]. In Eq. (5), the function

$$S_{WS}(k)=k^2/(k^2+q_{WS}^2) \tag{7}$$

represents the renormalized screening factor derived on the basis of the Wigner-Seitz sphere model of the strongly coupled electron system; the screening parameter q_{WS}, which scales as the inverse of the Wigner-Seitz sphere radius, has been evaluated in II. Significance of adopting such a Wigner-Seitz sphere model in strongly coupled plasmas has been elucidated through various examples.[25,27–29]

The collision time $\tau(q)$ due to Coulomb scattering between electrons is calculated as [cf. Eq. (4.14) in I]

$$\frac{1}{\omega_p\tau(q)}=-\frac{1}{N}\sum_{k\neq\vec{0},\vec{q}}K(\vec{q},\vec{k})\frac{\pi q_{FT}\theta(2q_F-k)}{2\sqrt{3}k}[S_{WS}(k)]^2\times[S(|\vec{k}-\vec{q}|)-S_{HF}(|\vec{k}-\vec{q}|)]\ . \tag{8}$$

Here $\omega_p=(4\pi ne^2/m)^{1/2}$ is the plasma frequency; $\theta(x)$, the unit step function; $q_{FT}=\sqrt{3}m\,\omega_p/\hbar q_F$, the Fermi-Thomas wave number; $q_F=(3\pi^2n)^{1/3}$, the Fermi wave number; and $n=N/V$, the average number density. Two important modifications from Eq. (4.14) in I are to be noted in (8). First, the screening factor $S_{WS}(k)$ in (7) is used in place of the Fermi-Thomas screening function $1/\epsilon_{FT}(k)$; this replacement is in accord with the Wigner-Seitz sphere model which we have adopted. Second, the effects of Coulomb correlations are measured in (8) as $[S(|\vec{k}-\vec{q}|)-S_{HF}(|\vec{k}-\vec{q}|)]$ rather than as $[S(|\vec{k}-\vec{q}|)-1]$. The strength of the Coulomb coupling is described by the usual r_s parameter,

$$r_s\equiv(3/4\pi n)^{1/3}me^2/\hbar^2\ . \tag{9}$$

As we have argued in II, in the limit of $r_s\to 0$, that is, when the Coulomb interaction is turned off, the Hartree-Fock correlation $S_{HF}(q)$ still remains; Eq. (8) takes this limiting behavior into account.

Since numerical values for $S(q)$ are available from the solution of the self-consistent integral equations described in II, we substitute those values in (8) to compute the relaxation rate; the results are shown in Fig. 1. As remarked in I, $1/\tau(q)$ is proportional to q^2 in the long-wavelength domain, reflecting the conser-

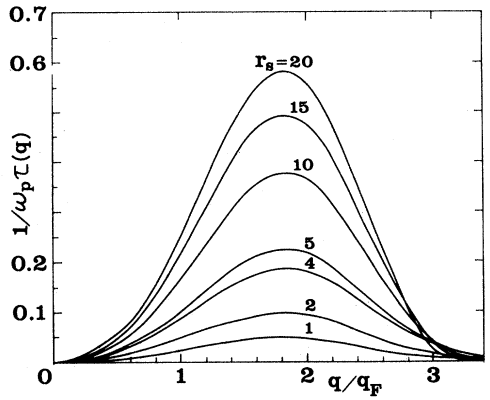

FIG. 1. Values of $1/\omega_p\tau(q)$ vs q/q_F for $r_s=1$, 2, 4, 5, 10, 15, and 20.

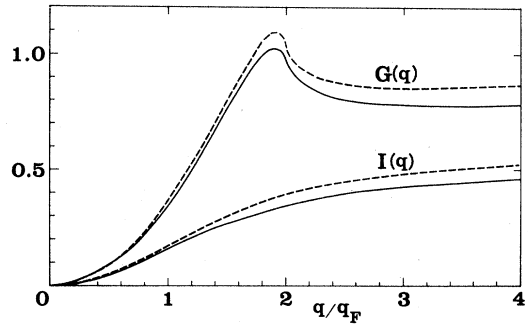

FIG. 2. Local-field corrections $G(q)$ and $I(q)$ vs q/q_F for $r_s=2$ (solid curves) and $r_s=4$ (dashed curves).

vation of the total momentum in the system. In the short-wavelength domain, $1/\tau(q)$ behaves as q^{-4} since $S(q)-S_{HF}(q)$ decays as q^{-4}. The relaxation rate $1/\tau(q)$ thus takes on a maximum value at $q\simeq 1.85\,q_F$.

In order to see the validity of the use of the screening function (7) and (8), we have separately computed the values of (8) where $S_{WS}(k)$ is now replaced by $\epsilon_{FT}(k)^{-1}=k^2/(k^2+q_{FT}^2)$. The numerical values so obtained turned out to be smaller by an order of magnitude than those given in Fig. 1, a tendency contradicting with the experimental indications as we shall see. Furthermore the computed values of $1/\tau(q)$ as a function of r_s first started to increase, but then tended to decrease drastically as r_s exceeded beyond 5. This is to be compared with the systematic variation exhibited in Fig. 1, which we take to be the more accurate evaluation.

The short-time relaxation frequency $\Omega(q)$ is determined in such a way that the dielectric function (2) satisfy the third frequency-moment sum rule. This requirement leads to the expression,

$$\Omega(q)/\omega_p=(\pi/2)^{1/2}\omega_p\tau(q)[G(q)-I(q)]\ , \quad (10)$$

where

$$I(q)=-\frac{1}{N}\sum_{k\neq\vec{q},0}K(\vec{q},\vec{k})\frac{\vec{k}\cdot\vec{q}}{q^2}\,[S(|\vec{q}-\vec{k}|)-1]\ . \quad (11)$$

As we have remarked in I, the functions, $G(q)$ and $I(q)$, correspond to the low- and high-frequency limits of the frequency-dependent local-field correction, respectively.

For the validity of the present theory we must make sure $G(q)\geq I(q)$ so that $\Omega(q)$ in (10) remains a positive definite quantity. The computed values of $G(q)$ and $I(q)$ at $r_s=2$ and 4 are plotted in Fig. 2. We find that the condition is satisfied in those cases. In the limit of $q\to 0$, $\Omega(q)$ takes on a finite value; in the limit of $q\to\infty$, $\Omega(q)$ behaves as q^4.

III. PLASMON DISPERSION AND LINEWIDTH

The critical wave number q_c is defined as that wave number at which the plasmon dispersion merges into the continuum of the single-pair excitations.[16] In the long-wavelength domain such that $q<q_c$, the plasmon suffers no Landau damping; it decays only through collisional processes. In the electron-liquid calculations as outlined in Sec. II, the decay rate of the plasmon would vanish in the long-wavelength limit since $1/\tau(q)$ is proportional to q^2. In actual metals, however, the linewidths of the plasmon spectra observed by scattering experiments[4,7,10,13] take on nonvanishing, finite values in the limit of $q\to 0$. This observation clearly indicates necessity of considering those additional scattering processes of electrons which would not conserve their total momentum; examples of such processes are the interband transitions, scattering with phonons, impurities, and so on.

Those extra scattering processes can be included in our formalism through addition of the corresponding decay term,

$$-i\frac{\hbar}{\tau_0(q)}\left[\rho_{\vec{p}\,\vec{q}}(t)+\frac{f_{\vec{p}}-f_{\vec{p}+\vec{q}}}{V\hbar\omega_{\vec{p}\,\vec{q}}\chi_0(q,0)}\rho_{\vec{q}}(t)\right]\ , \quad (12)$$

to the right-hand side of Eq. (3.7) in I, the equation of motion for the Wigner distribution function. The factor $1/\tau_0(q)$ in (12) describes the decay rate of the Wigner distribution due to those nonconserving scattering processes. In principle one would argue that the short-time relaxational effect described by a frequency $\Omega_0(q)$ should also be included in (12), as we did for the electron-electron interactions. By assuming $\omega_p\ll\Omega_0(q)$, however, we neglect this effect and thereby adopt (12).

From the equation of motion so modified, we find the dielectric response function which takes the same form as (2), with the definition of $\tilde{\omega}$ slightly altered as

$$\tilde{\omega}=\omega+\left(\frac{2}{\pi}\right)^{1/2}\frac{\Omega(q)}{\omega\tau(q)}\left[W\left(\frac{\omega}{\Omega(q)}\right)-1\right]+i\frac{1}{\tau_0(q)} \quad . \tag{13}$$

The plasmon pole $\omega=\omega(q)$ may then be determined from the equation, $\epsilon(q,\omega(q))=0$. We set its long-wavelength solution as

$$\omega(q)=\omega(0)+[2\alpha\omega_F-i\beta(\omega_p/2)](q/q_F)^2 \quad , \tag{14}$$

where

$$\omega(0)=\tilde{\omega}_p-i/2\tau_0(q) \quad , \tag{15}$$

$$\tilde{\omega}_p=\{\omega_p^2-[1/2\tau_0(q)]^2\}^{1/2} \quad , \tag{16}$$

and $\omega_F=\hbar q_F^2/2m$ is the Fermi frequency. The q dependence of $1/\tau_0(q)$ is still retained in the formal definitions of (15) and (16); in practical applications to be carried out later, however, we shall approximate it by the long-wavelength value $1/\tau_0(0)$.

The dispersion and decay coefficients, α and β, are defined by Eq. (14). Those may be given from the real and imaginary parts of the following equation:

$$2\alpha\omega_F-i\beta\frac{\omega_p}{2}=\frac{2\omega_F^2}{3\tilde{\omega}_p}+\frac{8\omega_F^2}{15\tilde{\omega}_p}\left[\frac{\omega(0)}{\omega_p}\right]^2-\frac{\omega_p^2}{2\tilde{\omega}_p}\left[\gamma_\infty(r_s)+[\gamma_0(r_s)-\gamma_\infty(r_s)]W\left(\frac{\omega(0)}{\Omega(0)}\right)\right] \quad . \tag{17}$$

Here $\gamma_0(r_s)$ and $\gamma_\infty(r_s)$ are the coefficients in the long-wavelength expressions for $G(q)$ and $I(q)$ such that[24]

$$\lim_{q\to 0} G(q)=\gamma_0(r_s)(q/q_F)^2 \quad , \tag{18}$$

$$\lim_{q\to 0} I(q)=\gamma_\infty(r_s)(q/q_F)^2 \quad . \tag{19}$$

Those coefficients are related, respectively, to the compressibility and the internal energy of the system; they are actually computed according to Eqs. (44) and (16) in II.

The linewidth associated with the excitation spectrum of the plasmon is twice the imaginary part of $\omega(q)$ in (14). In the long-wavelength limit, it then assumes the value $1/\tau_0(0)$. For each metal, this value can be determined from the plasmon linewidth observed experimentally. In the case of Al,[4,10,13] we may take $1/\omega_p\tau_0(0)=0.03$; for Na,[4] $1/\omega_p\tau_0(0)=0.07$. In our subsequent numerical computations concerning those metals, we ignore the possible q dependence of $1/\tau_0(q)$, which we shall simply write as $1/\tau_0$.

IV. NUMERICAL RESULTS AND COMPARISON WITH EXPERIMENTS

We now compute the dynamic structure factor according to (1) and compare the various features with the experimental data and other theories. We begin with the dispersion coefficient α evaluated in the electron-liquid model.

A. Dispersion coefficient α

In the electron-liquid model, one does not take account of those scattering processes which would destroy the conservation of the total momentum; hence, one sets $1/\tau_0(q)=0$ in Eq. (17). The dispersion coefficient in this model is, therefore,

$$\alpha=\alpha_{RPA}-\frac{\omega_p}{4\omega_F}\left[\gamma_\infty(r_s)+[\gamma_0(r_s)-\gamma_\infty(r_s)]\times \mathrm{Re}W\left(\frac{\omega_p}{\Omega(0)}\right)\right] \quad , \tag{20}$$

where

$$\alpha_{RPA}=3\omega_F/5\omega_p \tag{21}$$

is the dispersion coefficient evaluated in the RPA. As we observe in (20), the present formulation takes account of both static and dynamic strong-coupling effects in the dispersion coefficient, arising from the exchange and Coulomb correlations. The quantities, $\gamma_0(r_s)$ and $\gamma_\infty(r_s)$, stem from the static and high-frequency limits of the local-field correction; Eq. (20) then mixes those two contributions in the way determined by the frequency ratio $\omega_p/\Omega(0)$.

The expressions for α proposed in other existing theories may all be regarded as certain limiting cases of (20). For instance, if one disregards the relaxational effect in the short-time domain and thereby lets $\Omega(0)\to\infty$, then Eq. (20) reduces to

$$\alpha_0=\alpha_{RPA}-(\omega_p/4\omega_F)\gamma_0(r_s) \quad . \tag{22}$$

The expressions obtained by Singwi and his coworkers[30–32] and by Lowy and Brown[33] correspond to (22), although the numerical evaluations for $\gamma_0(r_s)$ are different from one theory to the other. Basically these are static theories and thus involve the static local-field correction represented by $\gamma_0(r_s)$.

In the weak-coupling limit of $r_s\to 0$, one retains the lowest-order contributions of the exchange effects only, and finds[25,34] $\gamma_0(0)=\frac{1}{4}$. In this limit, Eq. (22)

becomes

$$\alpha_{TW} = \alpha_{RPA} - \omega_p/16\omega_F \ , \tag{23}$$

the expression derived by Toigo and Woodruff.[35]

If on the other hand one assumes that the plasmon has a sufficiently high energy so that an approximation $\omega_p/\Omega(0) \to \infty$ is applicable, then Eq. (20) reduces to

$$\alpha_\infty = \alpha_{RPA} - (\omega_p/4\omega_F)\gamma_\infty(r_s) \ . \tag{24}$$

This is the expression obtained by Pathak and Vashishta[36] and by Jindal *et al.*[19] These authors took account of the third frequency-moment sum rule, which is reflected in the involvement of $\gamma_\infty(r_s)$.

Finally one notes that the lowest-order exchange contributions to $\gamma_\infty(r_s)$ may be evaluated by going over to the weak-coupling limit, $r_s \to 0$, so that[24,32,36] $\gamma_\infty(0) = 3/20$. In this limit, one finds from Eq. (24)

$$\alpha_{NP} = \alpha_{RPA} - 3\omega_p/80\omega_F \ . \tag{25}$$

This expression was obtained by Nozières and Pines,[37] and by DuBois.[38]

For comparison the values of α/α_{RPA} as computed according to Eqs. (20) and (22)–(25) are shown in Fig. 3. In the computations we have used the values of $\gamma_0(r_s)$ and $\gamma_\infty(r_s)$ obtained in II. In Fig. 3 we have also plotted the experimental data reported by various investigators for various metals.[15] We may interpret those data as indicating collectively that the measured values for α are significantly different from the RPA prediction (21) and that the discrepancies widen as r_s increases. Since the measured values are rather widely scattered and are attached with large error bars, it does not appear feasible to decide which theoretical prediction, if any, fits the data most accurately. We here remark on the theoretical soundness of (20), since the other formulas are applicable only to certain limiting cases which may not correspond to real metallic situations.

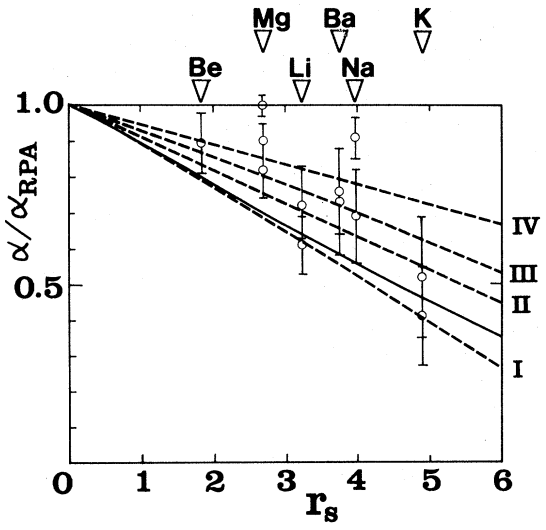

FIG. 3. Plasmon dispersion coefficient α divided by the RPA value α_{RPA} vs r_s in various approximations. Solid line corresponds to the present result, Eq. (20). Curves I–IV correspond to α_0, α_{TW}, α_∞, and α_{NP} in Eqs. (22)–(25), respectively. The experimental results for Be, Al, Mg, Li, Ba, Na, and K are taken from Ref. 15.

B. Dynamic structure factor

We have carried out detailed computations of the dynamic structure factor reduced to a dimensionless form,

$$\tilde{S}(q,\omega) = (2\pi\omega_F/3N)S(q,\omega) \ ,$$

at $r_s = 2$ and 4. The computations were performed according to (1), where four separate cases of the expression for $\epsilon(q,\omega)$ were treated. Each of those expressions represents a different degree of approximation as explained in the following:

a. Approximate description for the metallic electrons. This corresponds to the use of the dielectric function (2) with $\tilde{\omega}$ defined as (13). For $r_s = 2$, we take $1/\omega_p\tau_0(q) = 1/\omega_p\tau_0(0) = 0.03$, appropriate to Al; for $r_s = 4$, $1/\omega_p\tau_0(q) = 1/\omega_p\tau_0(0) = 0.07$, appropriate to Na.

b. Electron-liquid model. This amounts to assuming $1/\omega_p\tau_0(q) = 0$ in *a*.

c. Static approximation to the local-field correction. This further takes $1/\tau(q) = 0$ in *b*.

d. RPA. This is approached by letting $G(q) = 0$ in *c*.

Figures 4–7 illustrate some typical shapes of $\tilde{S}(q,\omega)$ at two values of q, one in $q < q_c$ and the other in $q > q_c$, for $r_s = 2$ and 4 in the four approximations listed above. Overall features of $\tilde{S}(q,\omega)$ obtained through those computations will be compared with the experimental results in the balance of this section. Here we note on some detailed character of the computed spectral functions.

Since the approximations *a* and *b* take account of the collisional effects, we find that the resulting spectra of the plasmon excitations have finite linewidths and that the entire spectral functions have tails extending beyond the frequency domain of the single-pair excitations. These features are the consequences of the multipair excitations.[16,24]

Platzman and Eisenberger[5] reported an experimental observation of double-peak structures in the excitation spectra of the electron liquids in Be, Al, and C over the wave-number domain of $1.13 < q/q_F < 2.10$. Such structures are not visible in the results of our computations. Mukhopadhyay, Kalia, and Singwi[22] and very recently Awa, Yasuhara, and Asahi[23] ad-

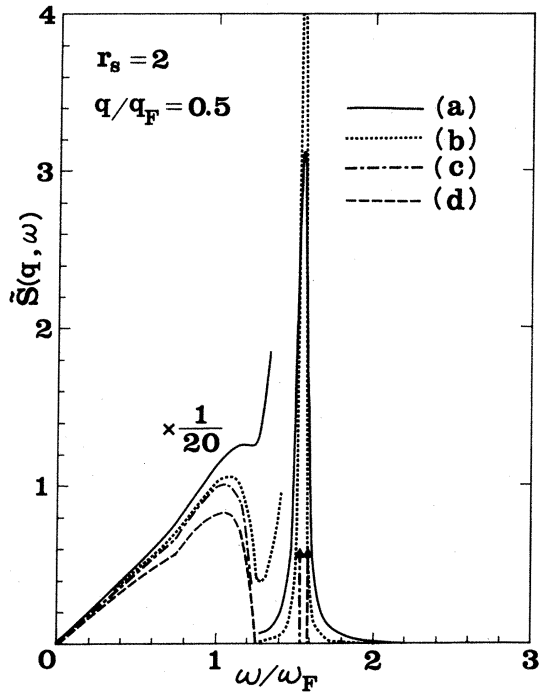

FIG. 4. Dynamic structure factor $\tilde{S}(q,\omega)$ vs ω/ω_F for $r_s = 2$ and $q/q_F = 0.5$ in the approximations $a-d$. Arrows indicate the δ functions corresponding to the plasmon excitations. In the low-frequency region, spectral functions of the single-pair-excitation continuum are magnified by 20 times.

vanced theoretical calculations capable of reproducing spectral shapes which qualitatively resemble parts of the observed structures. Those authors did so by taking account of the lifetime effect in the single-particle self-energy which acts to modify the Lindhard polarizability.

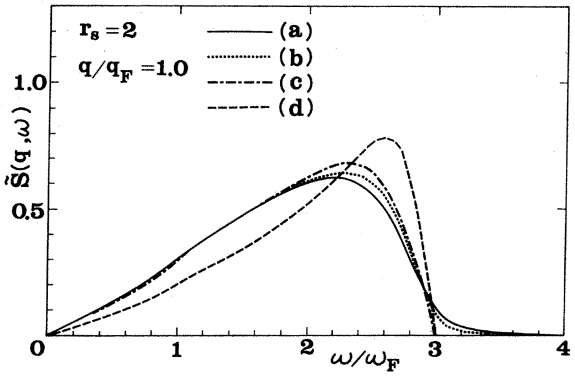

FIG. 5. Dynamic structure factor $\tilde{S}(q,\omega)$ vs ω/ω_F for $r_s = 2$ and $q/q_F = 1$ in the approximations $a-d$.

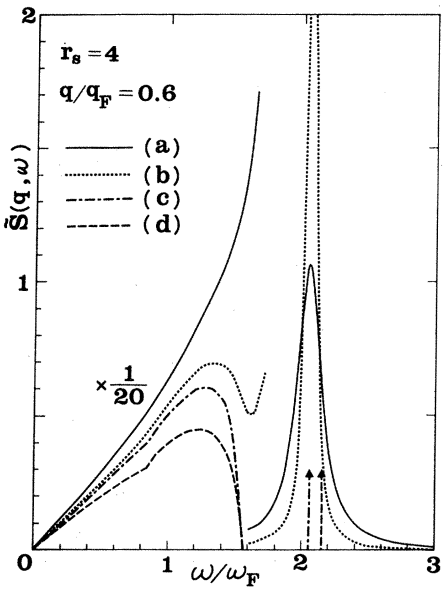

FIG. 6. Same as Fig. 4 with $r_s = 4$ and $q/q_F = 0.6$.

C. Plasmon dispersion curve

In the compilation of the experimental data in Fig. 3, we have not included the measured values of α for Al, one of the best studied metals as far as the plasmon dispersion is concerned. The reason is that different values of the dispersion coefficient have been reported for Al, depending on the ranges of the wave number studied. For instance, Krane[13] found $\alpha/\alpha_{RPA} \simeq 0.47$ in the range $0 < (q/q_F)^2 \lesssim 0.1$, and $\alpha/\alpha_{RPA} \simeq 1.0$ in the range $0.1 \lesssim (q/q_F)^2$. Obviously such a feature may exist for other metals as well; compilation of data such as in Fig. 3 must therefore be looked upon with this possibility in mind.

For the aluminum we therefore compare the dispersion curve of the plasmon peak between the

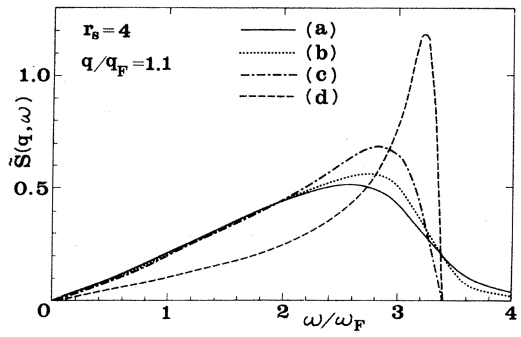

FIG. 7. Same as Fig. 5 with $r_s = 4$ and $q/q_F = 1.1$.

experimental data and the theoretical results. Such a comparison in the long-wavelength domain $q < q_c$ is shown in Fig. 8; the theoretical curves there are obtained with the approximations *a* and *d* in Sec. IV B.

It has been observed experimentally that the plasmon dispersion flattens as the wave number increases into the short-wavelength region $q > q_c$. This is a strong-coupling effect in the electron liquid, since a calculation based on the RPA theory does not account for such a flattening. Computed results of the dispersion curve in the short-wavelength region are shown in Figs. 9 and 10 for $r_s = 2$ and 4; the four curves in each figure correspond to the four approximation schemes, *a*–*d*, introduced in Sec. IV B. Experimental values for Al obtained by various investigators[6,7,10,11] are also plotted in Fig. 9. The local-field correction arising from the short-range static correlations, which is included in the scheme *c*, already shows a substantial effect in lowering the plasmon energy and flattening its dispersion over the RPA values. This tendency becomes more pronounced as we proceed to include the dynamic local-field effects in *a* and *b*. Improved agreement with the experimental indications appears to be obtained when those dynamic effects are taken into account. It is also notable that a negative dispersion is predicted for $r_s = 4$.

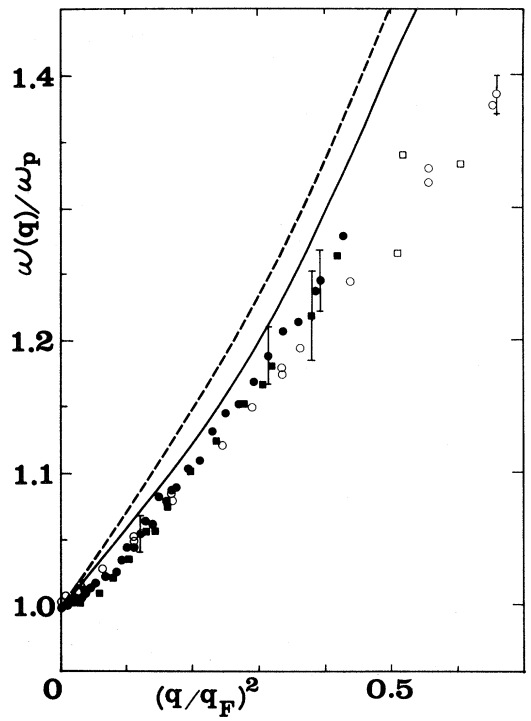

FIG. 8. Normalized plasmon dispersion curves vs $(q/q_F)^2$ for $r_s = 2$. Solid line is the result of the present work [scheme *a* in Sec. IV B]; dashed line, that in the RPA. Points are the experimental results for Al taken from Ref. 4 (solid squares), Ref. 8 (open circles), Ref. 10 (open squares), and Ref. 13 (solid circles). Here we adopt the values, $\hbar\omega_p = 14.19$ eV and $q_F = 1.75$ Å^{-1}.

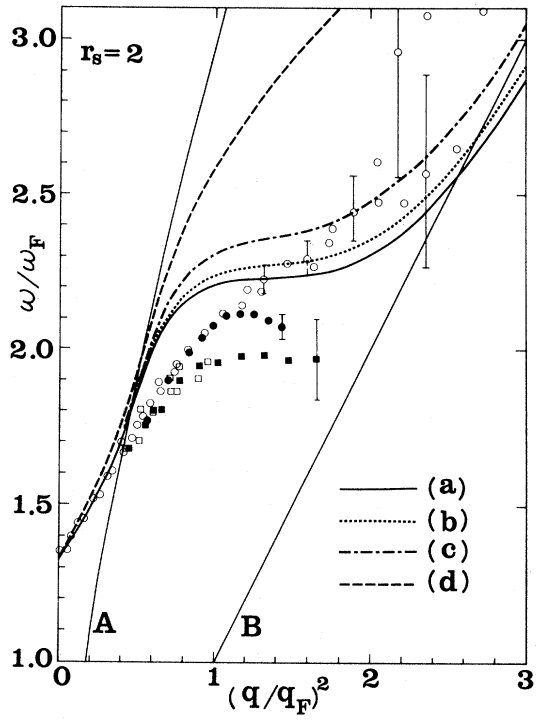

FIG. 9. Plasmon dispersion curves vs $(q/q_F)^2$ in the approximations *a*–*d* for $r_s = 2$. The line *A* represents the boundary of the single-pair-excitation continuum, $\omega/\omega_F = 2(q/q_F) + (q/q_F)^2$; and the line *B* refers to the peak frequency of the dynamic structure factor in the noninteracting case, $\omega/\omega_F = (q/q_F)^2$. Experimental results for Al are taken from Ref. 6 (solid circles), Ref. 7 (solid squares), Ref. 10 (open squares), and Ref. 11 (open circles).

D. Asymmetry in the peak structure of $S(q, \omega)$ for $q > q_c$

In the short-wavelength domain such that $q > q_c$, the plasmon peak merges into the continuum of the single-pair excitations; the peak structure of $S(q, \omega)$ exhibits an asymmetric character. Such an asymmetric behavior has been specifically monitored for Al in the experiment carried out by Gibbons *et al.*[10] They measured the average frequency between the two half-maximum frequencies of $S(q, \omega)$ and compared it with the peak frequency. To make contact with their experimental result, we have computed those two — average and peak — frequencies for $r_s = 2$ and 4 according to the scheme *a* in Sec. IV B. The computed results for $r_s = 2$ together with the experimental values[10] for Al are shown in Fig. 11.

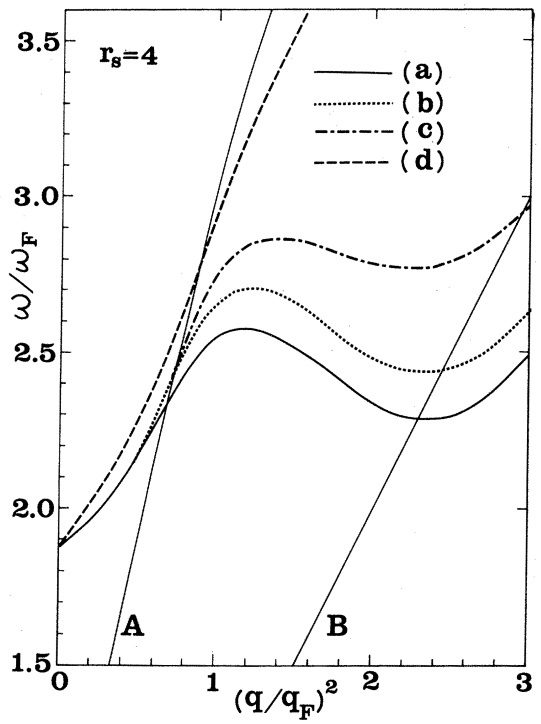

FIG. 10. Same as Fig. 9 with $r_s = 4$.

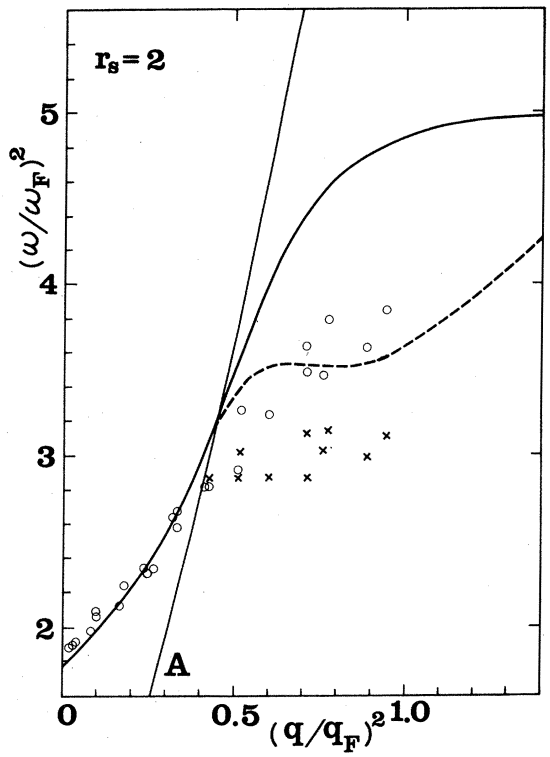

FIG. 11. Peak frequency and the average frequency between two half-maximum frequencies of $S(q,\omega)$ vs $(q/q_F)^2$ for $r_s = 2$ in the scheme *a*. The solid line represents the peak frequency; dashed curve, the average frequency. The line *A* refers to the boundary of the single-pair-excitation continuum. Experimental results for Al are taken from Ref. 10: open circles represents the peak frequency; crosses, the average frequency.

Although not shown in the figure, the computed value of the average frequency turns out greater than that of the peak frequency for $q > 1.35\,q_F$.

E. Full width at half maximum of the plasmon peak

The full width at half maximum, $w(q)$, of the plasmon peak measures the decay rate of the plasmon. We have computed this quantity for $r_s = 2$ and 4 in the four approximation schemes, $a-d$, described in Sec. IV B. Figure 12 shows the computed results for $r_s = 2$ and the experimental values[7,10] for Al. The major cause of the discrepancy between the present calculation and the experiment may be attributed to the adopted assumption $1/\tau_0(q) = 1/\tau_0(0)$, which fails to account for the q dependence inherent in those scattering processes contributing to $1/\tau_0(q)$. It has been theoretically shown by Sturm[39] that the interband transitions may make major contributions to the plasmon linewidth and its q dependence.

In the long-wavelength region, the numerical values of the linewidth calculated from (17) are

$$\frac{w(q)}{\omega_p} = \begin{cases} 0.03 + 0.057(q/q_F)^2, & 1/\omega_p\tau_0 = 0.03 \\ 0.039(q/q_F)^2, & 1/\omega_p\tau_0 = 0 \end{cases}, \tag{26}$$

for $r_s = 2$, and

$$\frac{w(q)}{\omega_p} = \begin{cases} 0.07 + 0.086(q/q_F)^2, & 1/\omega_p\tau_0 = 0.07 \\ 0.063(q/q_F)^2, & 1/\omega_p\tau_0 = 0 \end{cases}, \tag{27}$$

for $r_s = 4$. DuBois and Kivelson[18] calculated the plasmon linewidth by a diagramatic method and obtained

$$w(q)/\omega_p = 0.037(q/q_F)^2 \tag{28}$$

for Al; this essentially agrees with the second line of (26).

Gibbons *et al.*[10] on the other hand summarized

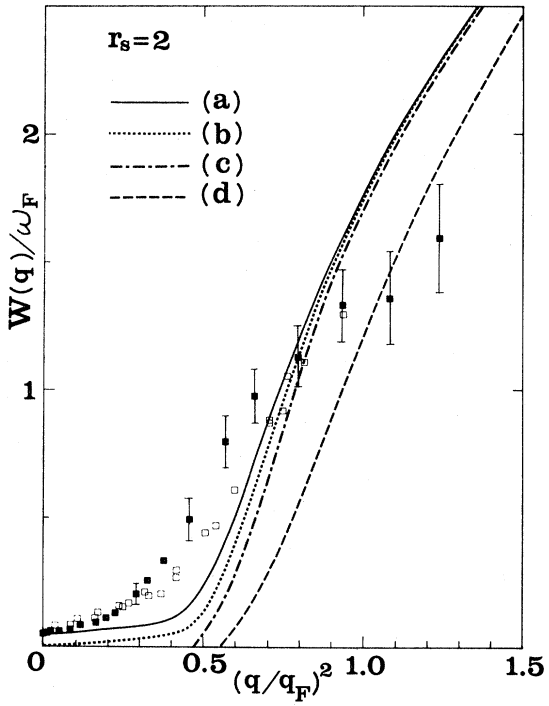

FIG. 12. Full width at half maximum, $w(q)$ vs $(q/q_F)^2$ for $r_s=2$ in the schemes $a-d$. Experimental results for Al are taken from Ref. 7 (solid squares) and Ref. 10 (open squares).

their experimental findings for Al into a formula,

$$w(q)/\omega_p = 0.034 + 0.50(q/q_F)^2 \ . \tag{29}$$

We may conclude from a comparison between (26) and (29) that the electron-electron interaction in the electron liquid provides only a minor contribution to the plasmon decay processes in actual crystalline metals.

V. SUMMARY

Following the general dielectric formulation and the numerical solution to the static structure factor, which were developed and obtained in the preceding two papers[24,25] for the strongly coupled electron liquid, we have numerically calculated the dynamic structure factor for $r_s=2$ and 4, with various degrees of approximation enumerated in Sec. IV B. Those results have been compared with the experimental data obtained for Al and other metals. The specific points of comparison were the plasmon dispersion curve both below and above the critical wave number, the plasmon linewidth, and the shape of the excitation spectrum. We have also derived a theoretical expression (20) for the plasmon dispersion coefficient, which encompasses many of the existing formulas as its limiting cases.

The numerical results in this formulation appear to show a fairly improved agreement with the experimental indications, as far as the overall features in the plasmon line and the excitation spectrum are concerned. The theory, however, is not capable of accounting for the double-peak structure in the excitation spectrum which was found in some experiments.

ACKNOWLEDGMENTS

We wish to thank Professor D. Pines for encouragement, Dr. H. Yasuhara for useful conversation and sending us their paper (Ref. 23) prior to publication, and the members of our research group for stimulating discussions. The numerical computations were carried out at the Computer Center of the University of Tokyo.

[1]H. Watanabe, J. Phys. Soc. Jpn. 11, 112 (1956).
[2]P. Schmüser, Z. Phys. 180, 105 (1964).
[3]C. Kunz, Z. Phys. 196, 311 (1966).
[4]T. Kloos, Z. Phys. 265, 225 (1973).
[5]P. M. Platzman and P. Eisenberger, Phys. Rev. Lett. 33, 152 (1974).
[6]H. J. Höberger, A. Otto, and E. Petri, Solid State Commun. 16, 175 (1975).
[7]P. Zacharias, J. Phys. F 5, 645 (1975).
[8]E. Petri and A. Otto, Phys. Rev. Lett. 34, 1283 (1975).
[9]J. Langkowski, J. Phys. D 8, 2058 (1975).
[10]P. C. Gibbons, S. E. Schnatterly, J. J. Ritsko, and J. R. Fields, Phys. Rev. B 13, 2451 (1976).
[11]P. E. Batson, C. H. Chen, and J. Silcox, Phys. Rev. Lett. 37, 937 (1976).
[12]C. H. Chen, J. Phys. C 9, L321 (1976).
[13]K. J. Krane, J. Phys. F 8, 2133 (1978).
[14]D. Pines, Rev. Mod. Phys. 28, 184 (1956); references to earlier theories and experiments may also be found here.
[15]H. Raether, *Excitations of Plasmons and Interband Transitions by Electrons* (Springer-Verlag, Berlin, 1980); further references to recent experiments may also be found here.
[16]D. Pines and P. Nozières, *The Theory of Quantum Liquids* (Benjamin, New York, 1966), Vol. I.
[17]For a review on the RPA approach, see, e.g., Ref. 16.
[18]D. F. DuBois and M. G. Kivelson, Phys. Rev. 186, 409 (1969).
[19]V. K. Jindal, H. B. Singh, and K. N. Pathak, Phys. Rev. B 15, 252 (1977).
[20]A. K. Gupta, P. K. Aravind, and K. S. Singwi, Solid State

Commun. 26, 49 (1978).
[21]G. Mukhopadhyay and A. Sjölander, Phys. Rev. B 17, 3589 (1978).
[22]G. Mukhopadhyay, R. K. Kalia, and K. S. Singwi, Phys. Rev. Lett. 34, 950 (1975).
[23]K. Awa, H. Yasuhara, and T. Asahi (unpublished).
[24]K. Utsumi and S. Ichimaru, Phys. Rev. B 22, 1522 (1980).
[25]K. Utsumi and S. Ichimaru, Phys. Rev. B 22, 5203 (1980).
[26]J. Lindhard, K. Dan. Vidensk. Selsk. Mat-Fys. Medd. 28, No. 8 (1954).
[27]H. E. DeWitt and Y. Rosenfeld, Phys. Lett. A 75, 79 (1979).
[28]N. Itoh and S. Ichimaru, Phys. Rev. A 22, 1318 (1980).
[29]K. Tago, K. Utsumi, and S. Ichimaru, Prog. Theor. Phys. 65, 54 (1981).
[30]K. S. Singwi, M. P. Tosi, R. H. Land, and A. Sjölander, Phys. Rev. 176, 589 (1968).
[31]K. S. Singwi, A. Sjölander, M. P. Tosi, and R. H. Land, Phys. Rev. B 1, 1044 (1970).
[32]P. Vashishta and K. S. Singwi, Phys. Rev. B 6, 875 (1972).
[33]D. N. Lowy and G. E. Brown, Phys. Rev. 12, 2138 (1975).
[34]L. J. Sham, Phys. Rev. B 7, 4357 (1973).
[35]F. Toigo and T. O. Woodruff, Phys. Rev. B 2, 3958 (1970); 4, 371, 4312 (1971).
[36]K. N. Pathak and P. Vashishta, Phys. Rev. B 7, 3649 (1973).
[37]P. Nozières and D. Pines, Phys. Rev. 111, 442 (1958).
[38]D. F. DuBois, Ann. Phys. (N.Y.) 8, 24 (1959).
[39]K. Sturm, Z. Phys. B 28, 1 (1977).